J Mater Sci (2008) 43:5211–5221
DOI 10.1007/s10853-008-2757-0

The development of voidage and capillary size within extruded plastic films

D. I. Medina · B. Hallmark · T. D. Lord · M. R. Mackley

Received: 5 March 2008 / Accepted: 28 May 2008 / Published online: 17 June 2008

Abstract This paper describes how both capillary diameter and voidage can be manipulated by downstream mechanical processing of plastic microcapillary films (MCFs). MCFs are a novel thermoplastic extrudate that have been manufactured by the entrainment of gas within nozzles positioned in an extrusion die; the film resembles a plastic tape but contains an array of equally spaced parallel microcapillaries that run along its entire length. The low-voidage MCFs manufactured from linear low density polyethylene were made by melt drawing the polymer to produce an essentially isotropic MCF. This MCF could then be subsequently mechanically drawn to form small diameter MCFs. By altering process conditions an anisotropic high voidage MCF was produced. This MCF was brittle when drawn in the capillary direction but showed unusual mechanical transverse drawing. The paper presents experiment details for the manufacture of the different MCF structures together with mechanical properties and X-ray orientation data. From this, qualitative explanations for the mechanisms to achieve the different structures are given.

Introduction

The manufacture of microcapillary films (MCFs) was first reported by Hallmark et al. [1]. MCFs contain an array of continuous hollow microcapillaries encapsulated within a thin polymer film. MCFs have certain properties similar to those of plastic film [2–4], hollow fibres [5–7] and closed-cell polymer foam [8, 9]. MCFs are produced via an extrusion process where thermoplastic from a screw extruder is extruded within a specially designed extrusion die.

The first generation of MCFs were termed "*low-voidage*" MCF. These materials were characterised as having essentially uniform capillaries and voidage typically between 10% and 15% based on the ratio of total capillary area to total polymer cross-sectional area, as shown in Fig. 1. The high accuracy of the features within a low-voidage MCF can be attributed to a carefully designed and precision fabricated die assembly. The low-voidage MCF product has capillary mean hydraulic diameters between 100 and 400 μm. The cross-sectional photomicrograph of the MCF shown in Fig. 1 has capillary mean hydraulic diameters of approximately 200 μm and was made with a commercially available grade of linear low density polyethylene (LLDPE), manufactured by the Dow Chemical Company Inc. (Dowlex NG5056G). The mechanism controlling the formation of low-voidage MCF is described in [1].

Alteration of process conditions can strongly influence the MCF's cross-sectional geometry and the capillary mean hydraulic diameters [10]. The low-voidage MCF existing range of diameters and geometries has certain advantages for applications such as microreactors [11]. In microreactor technology, it was demonstrated that MCFs are able to perform continuous flow reactions in devices constructed from low-voidage MCF called microcapillary flow discs (MFDs) [11]. The advantages of these MFDs are their low-cost, disposability, their support for high pressures and their ability to perform reactions for micro- and mesoscale flow chemistry. MCFs have also proved to be useful in microheat exchange applications. According to Hornung et al. [12], the heat transfer performance of MCF-based

D. I. Medina · B. Hallmark · T. D. Lord · M. R. Mackley (✉)
Department of Chemical Engineering, University of Cambridge, Pembroke Street, Cambridge CB2 3RA, UK
e-mail: mrm5@cam.ac.uk

Fig. 1 Photomicrograph of the 19-capillary low-voidage MCF extruded from linear low-density polyethylene with capillary mean hydraulic diameters approximately 200 μm

heat exchange devices is comparable with existing designs of copper-based microscale heat exchangers [13].

Downstream manipulation of normal polymer films has, in general, been extensively investigated in the past particularly in relation to the development of molecular orientation; see for example [14]. As such, a large body of literature on film extrusion, film casting and fibre spinning is of relevance to MCFs. Thin film extrusion is often carried out using an annular die. This process, termed film blowing, involves the polymer melt being extruded through an annular die to form a continuous tube. The tube is inflated by air pressure applied at the centre of the annular die, resulting in the tube being stretched simultaneously in two directions; see for example Han et al. [3]. The film is under tension, due to the nip rolls, which causes axial drawing while the air pressure inside the bubble generates the circumferential drawing [4]. In order to obtain a consistent width and thickness of the film during the expansion of the bubble, the air flow conditions such as pressure are controlled during the process [2]. The freeze line, defined as the point where solidification starts, determines both the mechanical and optical properties [2, 4].

Film casting is an alternative method of forming polymer films. The molten polymer is extruded through a slit-die and is stretched in air before being cooled on a chill roll. Subsequently, the polymer film can be stretched under controlled conditions in the solid state [2, 15].

Downstream drawing of polymer films has been found to alter not only the physical shape and form of the product, but also to change the polymer's mechanical properties. The change in elastic and other mechanical properties due to a drawing process is mainly a consequence of the molecular orientation within the polymer [14].

Melt drawing is another route for obtaining highly oriented film products. By this method, it is possible to achieve high extension moduli and strengths, via flow-induced chain extension and solid state drawing [16]. Drawing in the solid state has been extensively studied [17–19]. The physical and mechanical properties of solid-phase polyethylene depend strongly on both its molecular architecture [20] and on the manner in which it was produced.

In this paper, downstream mechanical drawing techniques have been applied to obtain a range of new MCF microstructures. A *small diameter low-voidage MCF* was manufactured by the mechanical drawing of a standard-low voidage MCF and both X-ray and mechanical properties established. The addition of gas injection and cooling has been applied to create a new *high-voidage MCF*. Orientation within the MCF is captured within the solid product thereby producing an intrinsically anisotropic material. The high-voidage MCF has a mean hydraulic diameter of up to around 700 μm and again X-ray and mechanical properties were investigated. The high voidage MCF was found to be highly anisotropic and it was discovered that transverse drawing of the high-voidage MCF could produce an unexpected *ultra-high voidage MCF*.

The paper describes the range of MCF microstructures, namely low-voidage, small diameter low-voidage, high voidage and ultra-high voidage, and data is interpreted in relation to both orientation and mechanical properties.

Experimental processing of MCFs and measurement of MCF products

The low-voidage MCF process

Low-voidage MCFs were made by an extrusion process [1, 10]. The basic process is shown in Fig. 2. Polymer is fed into a single-screw extruder, which is connected to a gear pump. The molten polymer passes through a heated die with a convergent die-land where air is strategically entrained into the extrudate via an array of nozzles whose exits are coincident with the die exit. Once the extrudate exits the extrusion die, it is taken through a set of chilled rollers placed 35 mm from the die; this length is termed the melt drawing length. When the extrudate had been quenched, it was hauled off without further draw down. In this process, the melt drawing length and draw ratio (the ratio of the chill roll surface velocity to the velocity of the polymer at the die exit) could be manipulated to alter the size, shape and shape distribution of the capillaries, which could be either circular or elliptical in cross section. Using a carefully chosen set of conditions, low-voidage MCF with essentially uniform capillary size was obtained. The LLDPE used in the experimental part of this research is of commercially available grade (Dowlex NG5056G).

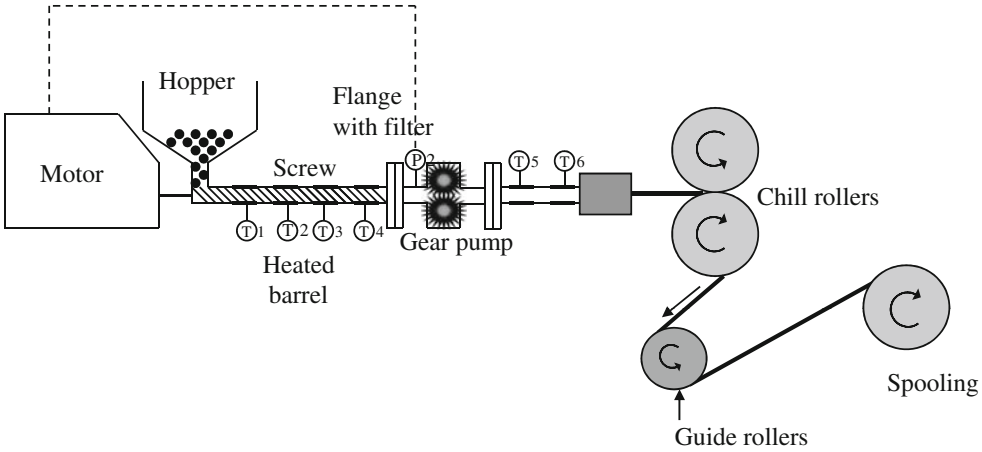

Fig. 2 Schematic diagram of the low-voidage MCF extrusion process

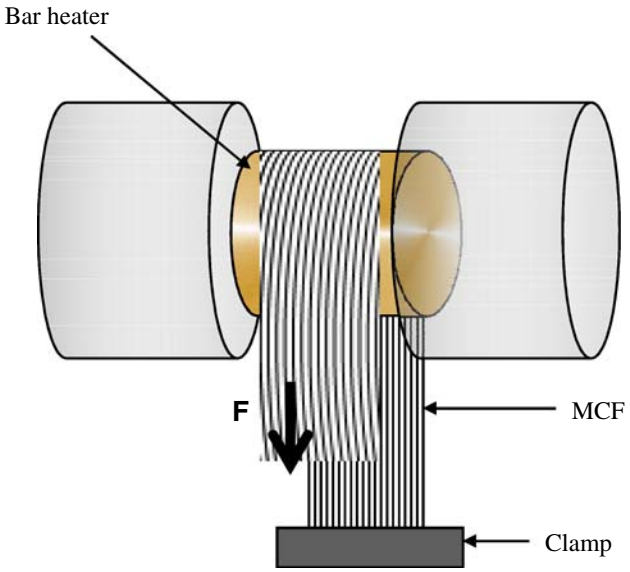

Fig. 3 Schematic diagram of the batch hot-drawing equipment

Small diameter low-voidage process

In order to decrease the capillary mean hydraulic diameter of the low-voidage MCF, a batch process, shown in Fig. 3, using LLDPE was first used to establish suitable drawing conditions. Subsequently, two strategies implementing continuous processing were used to attain a decrease in capillary diameter. In order to obtain a stable process for fabricating LLDPE film of small dimensions, a second hot drawing stage was necessary as shown in Fig. 4. This process differs from the low-voidage process in that after the chill rollers a guide roll was heated to a specific temperature, which was close to the melting temperature of the polymer (114 °C). The draw roller was held at room temperature and was set a velocity higher than the first chill roll velocity. In addition polyetherurethane (PEU), manufactured by BASF group (Elastollan 1185 A 10), was found experimentally to draw more easily than polyethylene and a series of melt drawn samples are reported for this material.

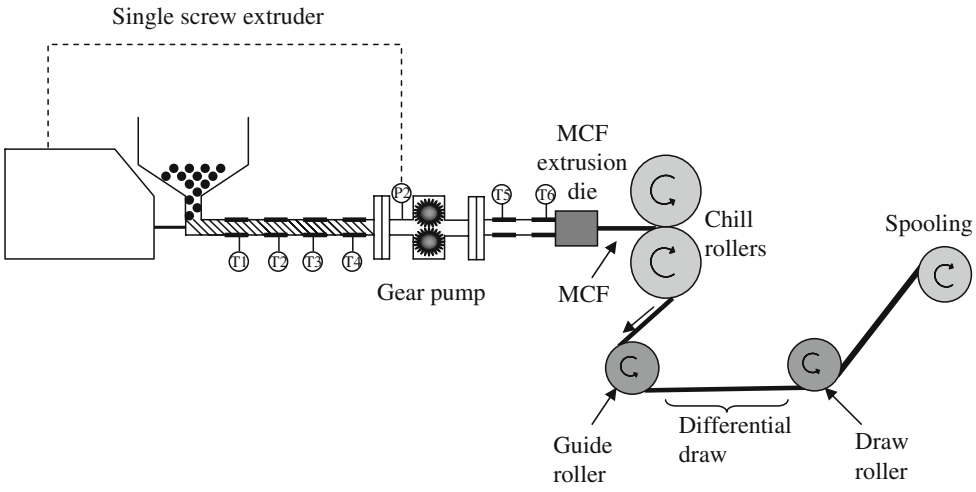

Fig. 4 Schematic diagram of the continuous small diameter low-voidage MCF extrusion process

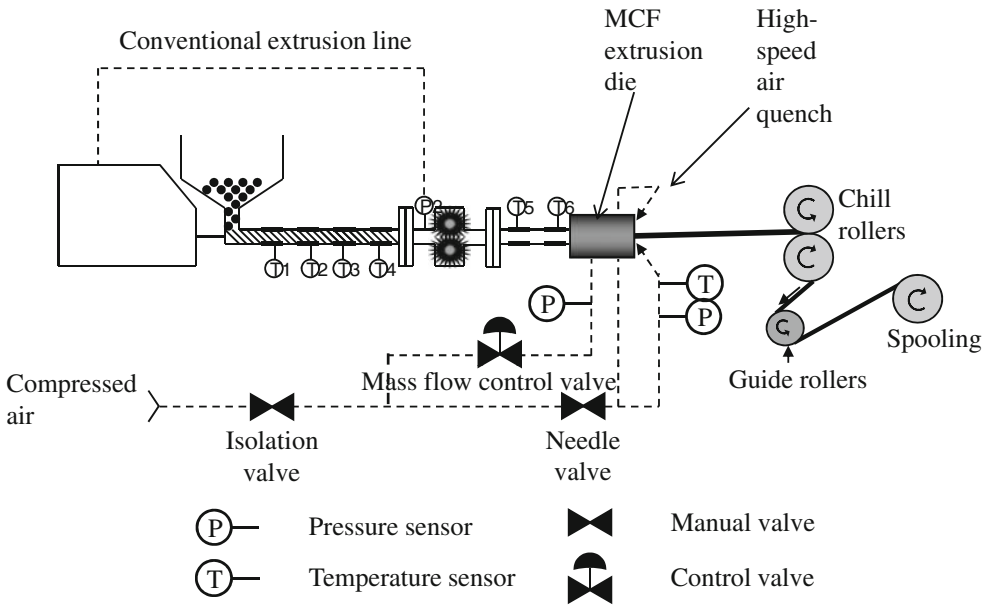

Fig. 5 Schematic diagram of the continuous high-voidage MCF process

High-voidage and ultra-high voidage MCF process

The manufacturing process for high-voidage MCF is illustrated in Fig. 5; the majority of the process hardware remains unchanged from the low-voidage case. A key difference, however, was the addition of a high-speed air quench in the form of two opposing air jets placed in a position that could quench the film as soon as it exited the die, and also a regulated gas supply was connected to the array of entrainment nozzles which could add a small amount of internal pressure to the capillaries, thus inflating them in a controlled manner. The initial compressed air supply was at approximately 750 kPa, and this supply was used for both the air quench and, after regulation to less than 110 kPa, to optionally supply the entrainment nozzles. Air pressure and temperature at the quench were monitored, and mass flow and pressure into the injectors were controlled [21].

Ultra-high voidage MCF was manufactured from high-voidage MCF by mechanically drawing the high-voidage MCF transverse to the capillary direction in a manner described in a later section of the paper.

Characterisation of MCF structures

Mechanical properties evaluation and ultra-high voidage manufacture

Evaluation of the tensile properties of both low- and high-voidage MCF was carried out using a stable microsystems texture analyser. The MCF was held between two clamps, orientated either horizontally or vertically. The MCF sample was clamped vertically to apply the load in the capillary direction (Fig. 6a) or horizontally to be drawn in the transverse direction (Fig. 6b). The top clamp was set to advance at a certain speed and load was recorded by the software TA Texture Expert, running on a PC. The bottom clamp remained stationary; the initial distance between the clamps was 10 mm.

Visual characterisation of MCF

The capillary dimensions and wall thickness were measured with an optical microscope (Olympus BH-2) equipped with a CCD camera and these results were supplemented by scanning electron microscopy (SEM) using a JEOL 6340F.

X-ray analysis

X-ray diffraction experiments were conducted to quantify the level of polymer orientation within different MCFs. A Bruker D8 Advance Diffractometer with a laboratory CuKα radiation source with wavelength 1.54 Å was used. The unit was operated at 45 kV and 45 mA. Diffraction data was collected using a 2D GADDS Bruker detector. The resolution of the detector was 1024 × 1024 pixels where one pixel was equal to 112 μm.

Wide angle data was collected using a distance between sample and detector of 7 cm. Calibration was carried out using a paraffin wax standard. The MCF was loaded in a sample holder, shown schematically in Fig. 7, such that the film was perpendicular to the incident beam and parallel to the 2D detector. The exposure time was 20 s. Following collection of the data, the pattern was corrected for spatial

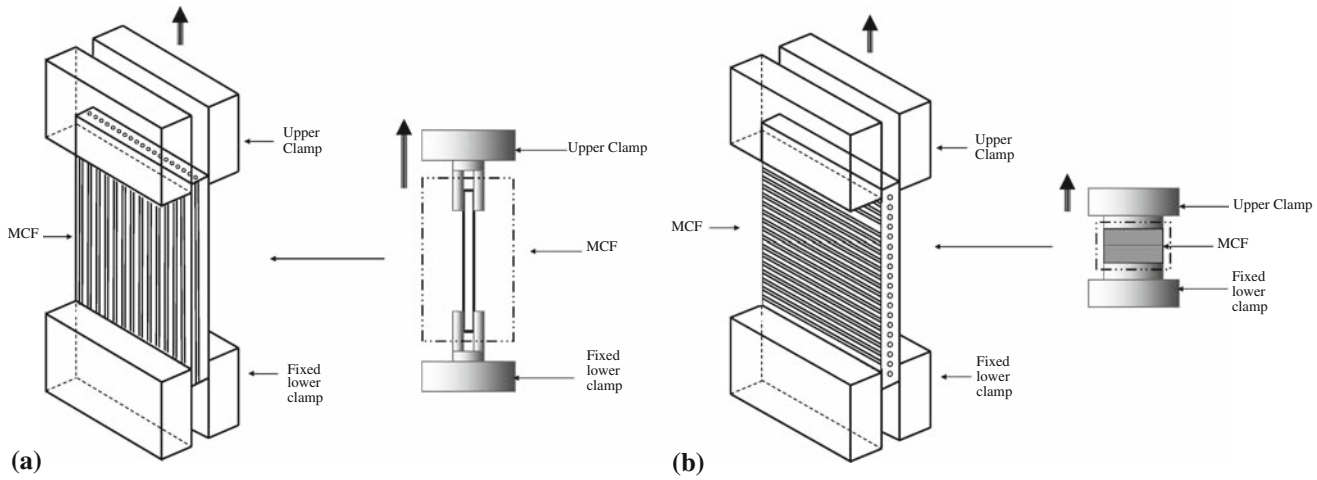

Fig. 6 Schematic diagrams showing (**a**) mechanical drawing along capillary axis, (**b**) mechanical drawing transverse to capillary axis

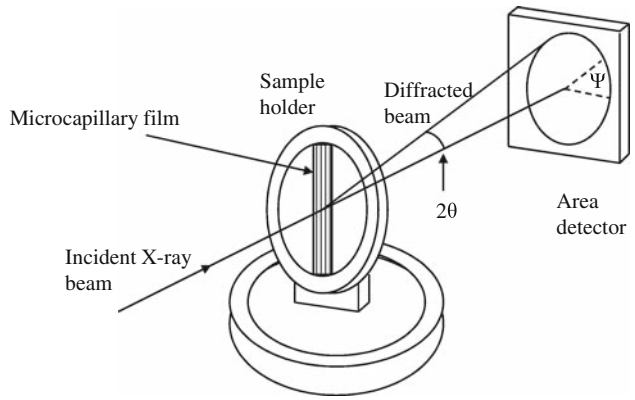

Fig. 7 Schematic diagram of the X-ray experimental set-up

distortion of the detector using a pre-determined spline function, with the intensities being normalised by using a measured flood field. This was done using software provided with the detector (BrukerAXS).

The diffraction data was analysed by using the Fit2D software [22]. The pattern was integrated radially to give a plot of intensity against azimuth angle. From this, the Herman orientation function was calculated. The diffraction patterns were indexed using the standard orthorhombic polyethylene structure, space group *Pnam* (number 62), at room temperature and pressure [23]. The first two reflections (110) and (200) were recorded in the data, and so the orientations along these crystallographic axes were calculated.

The degree of crystal orientation in the MCFs was characterised with the Hermans orientation functions, f_{110} and f_{200} [24, 25]:

The orientation function is defined as

$$f_{\mathrm{H}} \equiv \frac{3\langle \cos^2 \Psi \rangle - 1}{2} \tag{1}$$

with $\langle \cos^2 \Psi \rangle$ being defined as:

$$\langle \cos^2 \Psi \rangle \equiv \frac{\int_0^{\frac{\pi}{2}} I(\Psi) \cos^2 \Psi \sin \Psi \, \mathrm{d}\Psi}{\int_0^{\frac{\pi}{2}} I(\Psi) \sin \Psi \, \mathrm{d}\Psi} \tag{2}$$

where $I(\Psi)$ is defined as the intensity at azimuthal angle Ψ, measured from the assigned zero. When chains are perfectly aligned along the reference axis, $f_{\mathrm{H}} = 1$, whereas $f_{\mathrm{H}} = -1/2$ for chains aligned perpendicular to the reference axis. For random orientation, $f_{\mathrm{H}} = 0$.

Results

Microscopy, mechanical and X-ray characterisation of the different MCF structures were carried out. Mechanical measurements were made at a crosshead velocity of 5 mm/s for an initial sample length of 10 mm.

Low-voidage and small diameter low-voidage

A plot showing the room temperature mechanical drawing of low-voidage MCF is shown in Fig. 8. Initially the MCF

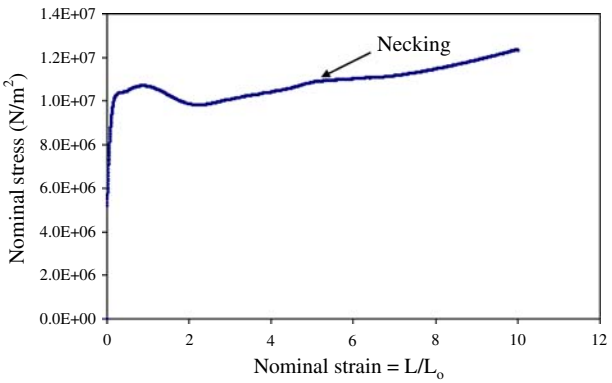

Fig. 8 Nominal stress–strain curve of the axial mechanical drawing of low voidage MCFs (initial sample length = 10 mm, crosshead velocity = 5 mm/s, temperature = 20 °C)

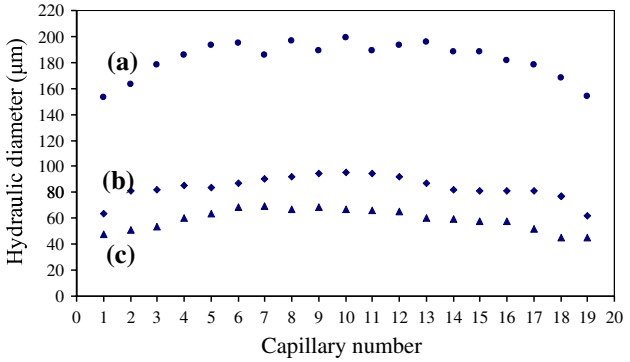

Fig. 9 Hydraulic diameter for individually numbered capillaries in a LLDPE MCF (**a**) low-voidage MCF, (**b**) small diameter low-voidage MCF and (**c**) small diameter low-voidage MCF after further deformation to rupture

draws elastically and then deforms plastically via a neck that propagates along the length of the sample. The drawing of the film causes a reduction of the size of the capillaries within the film as shown in Fig. 9. The development of orientation within the film is shown in Fig. 10. Figure 10a shows an initially low level of orientation within the film and Fig. 10b the development of orientation with subsequent mechanical drawing. Both (110) and (200) diffraction arcs show equatorial orientation and the value for the f_H orientation function for both initial and drawn MCF is shown in Table 1.

In order to achieve a higher draw ratio, hot drawing of LLDPE low-voidage MCF was also carried out, and the results for drawing at a temperature of 110 °C are shown in Fig. 11. In general, the reduction of hole diameter was consistent across the film as shown from the data in the figure, although the hole sizes near the outside edges of the film were less than the central hole size. Drawing conditions where a greater hole size reduction for LLDPE could not be found; however, it was discovered that by changing

Table 1 Orientation function for the (110) and (200) low-voidage LLDPE before and after deformation

Low-voidage			
Before drawing		After drawing	
Plane	Orientation function f_H	Plane	Orientation function f_H
(110)	0.29	(110)	0.83
(200)	0.13	(200)	0.80

the polymer to polyetherurethane (PEU), it was possible to reduce capillary size further.

Experimentally, it was found that PEU had a higher intrinsic drawability when compared to LLDPE. Data for a drawn PEU film is also shown in Fig. 11. A photomicrograph and a scanning electron micrograph of the near-micron-size micro-capillaries are shown in Fig. 12a and b.

The results presented show that the original melt cast MCF contains little orientation and consequently there is scope for further capillary hole size reduction and development of molecular orientation by the simple application of downstream mechanical drawing at either room temperature or elevated temperature.

High-voidage MCF and ultra-high voidage MCF

By modifying the process conditions, high-voidage MCF was manufactured and an optical micrograph of an example of these MCFs is given in Fig. 13. By using rapid quenching and higher nip-roll speeds it was possible to greatly increase the size of the capillary diameters. The individual diameter of capillaries within the MCF is shown in Fig. 14 and as with the low-voidage material the capillaries in the outer regions of the MCF have smaller diameter than in the central region. The X-ray diffraction pattern of the high-voidage MCF, shown in Fig. 15,

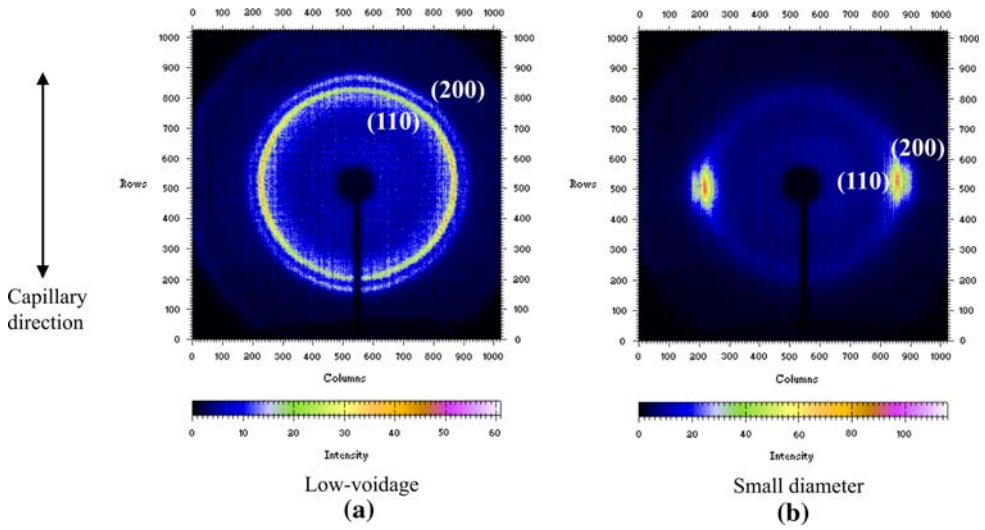

Fig. 10 WAXS pattern before and after the deformation for the mechanical drawing of low-voidage MCFs

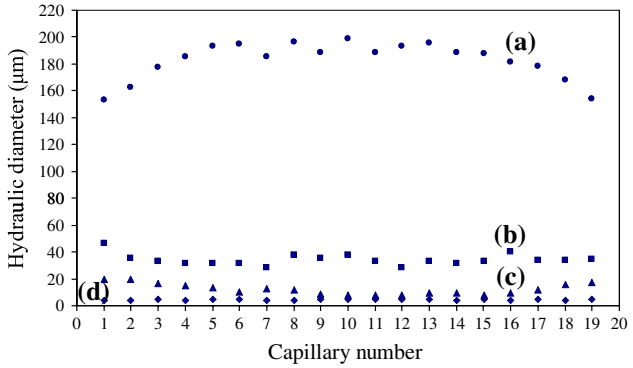

Fig. 11 Hydraulic diameter for individually numbered capillaries in (**a**) LLDPE low-voidage MCF, (**b**) continuous hot drawn LLDPE small diameter low-voidage MCF, (**c**) batch hot drawn LLDPE small diameter low-voidage MCF and (**d**) Continuous hot drawn PEU small diameter low-voidage MCF

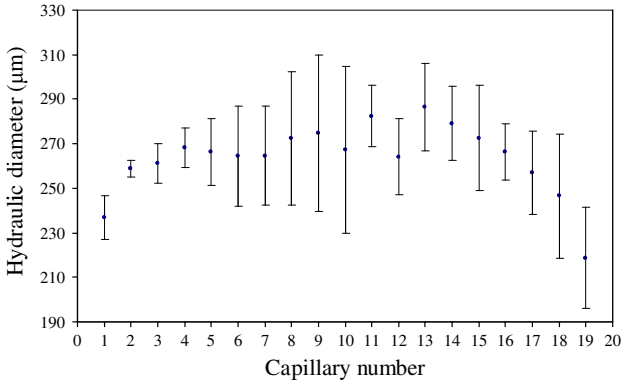

Fig. 14 Hydraulic diameter for individually numbered capillaries for high voidage MCFs

indicates in this case that there is orientation within the high-voidage MCF caused by the rapid quenching of the polymer as it exits the die. This orientation has a significant effect on the drawing characteristics of the film. Axial drawing, shown in Fig. 16, indicates that the material is essentially brittle and does not neck in the way that was found for low-voidage MCF. The magnitude of orientation both before and after drawing is shown in Table 2.

The high-voidage MCF showed an unusual draw behaviour when drawn transverse to the axial capillary direction. Figure 17 shows that the high-voidage MCF initially deforms in an essentially elastic way; however subsequently, individual thin wall microcapillary regions neck down causing a series of oscillations in the load deformation trace. The stress-strain oscillation corresponds to the successive necking of individual capillaries. In every case tested the first capillary to neck was the capillary nearest the moving crosshead. This then caused a cascade of necking, which was visualised optically in a time sequence of photographs shown in Fig. 18. This figure shows a progressive sequential necking of the capillary walls, which started from the top of the MCF. A schematic diagram indicating the formation of the transverse drawing of the MCF is shown in Fig. 19. The numbering in Fig. 19 is linked to the numbering in Fig. 17. For example the first stress oscillation (region 3) seen in Fig. 17 corresponds to the first necking of a microcapillary, indicated as 3 in Fig. 19. Further drawing results in further sequential necking, indicated as 4, n and F in Fig. 19.

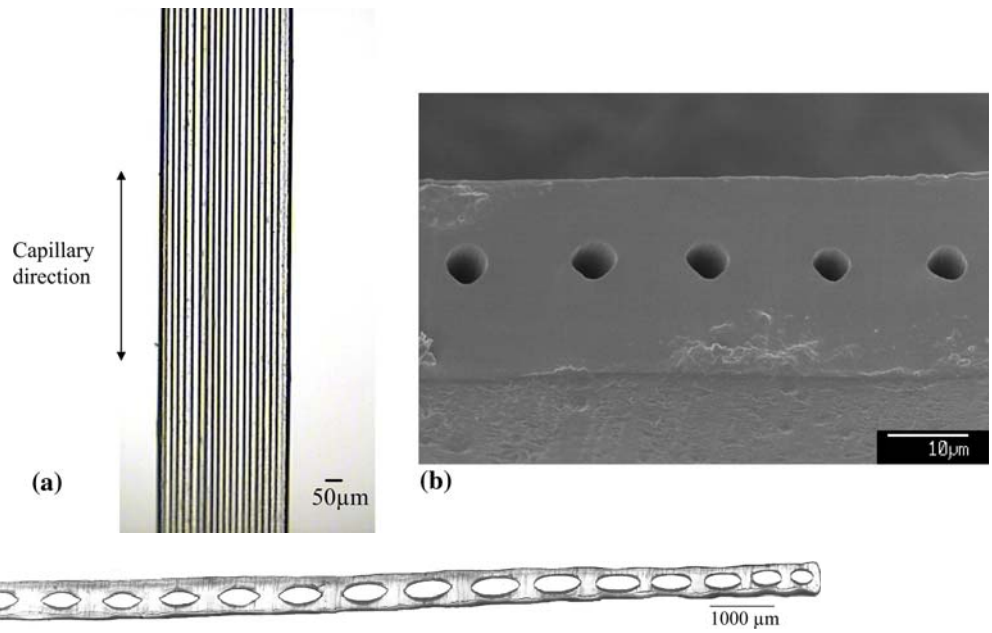

Fig. 12 Hot drawn PEU small diameter low-voidage MCF (**a**) optical micrograph showing good surface quality along length and (**b**) SEM showing transverse section with capillary mean hydraulic diameter of about 5 μm

Fig. 13 Optical cross-sectional view of high-voidage MCF with capillary mean hydraulic diameter approximately 250 μm

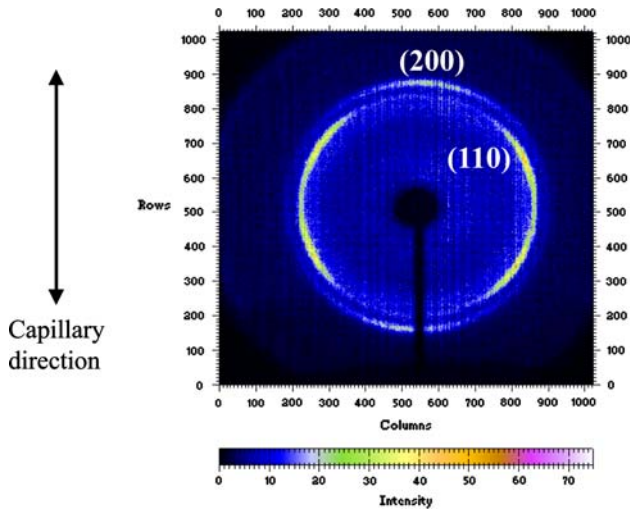

Fig. 15 Indexed WAXS pattern of high voidage MCFs

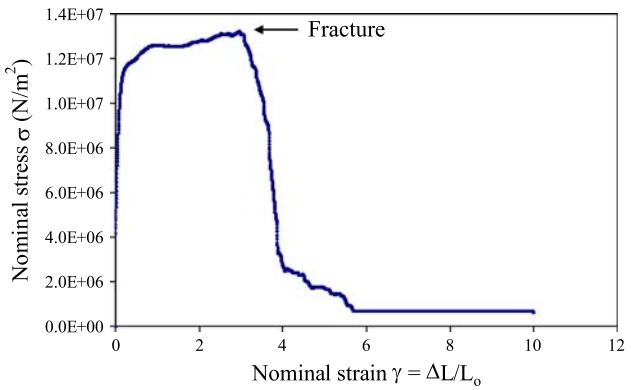

Fig. 16 Nominal stress–strain curve of the axial mechanical drawing of high-voidage MCF (initial sample length = 10 mm, crosshead velocity = 5 mm/s, temperature = 20 °C)

Table 2 Orientation function for the (110) and (200) high-voidage LLDPE before and after deformation

High-voidage			
Before drawing		After drawing	
Plane	Orientation function f_H	Plane	Orientation function f_H
(110)	0.27	(110)	0.38
(200)	−0.23	(200)	0.31

Optical and scanning electron micrograph of sections of the ultra-high voidage MCF are shown in Figs. 20 and 21; they show that very thin wall ultra-high voidage structures have been achieved. The mechanism controlling the deformation behaviour appears to relate to the intrinsic anisotropy of the film and its geometry. When transverse drawing is applied, stress levels will initially be highest in

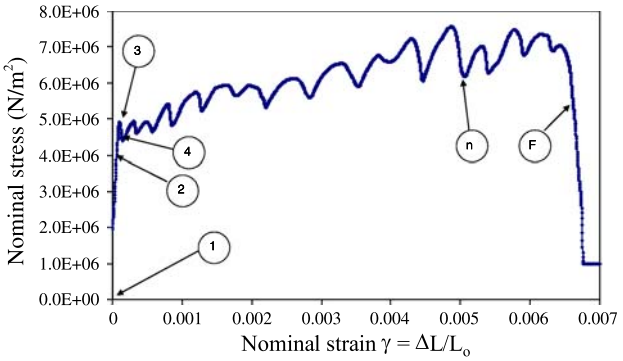

Fig. 17 Mechanical drawing for high-voidage MCF with deformation transverse to capillary direction showing successive necking of capillary walls and final necking of material between capillaries during the drawing process. Positions 1-F shown in Fig. 19

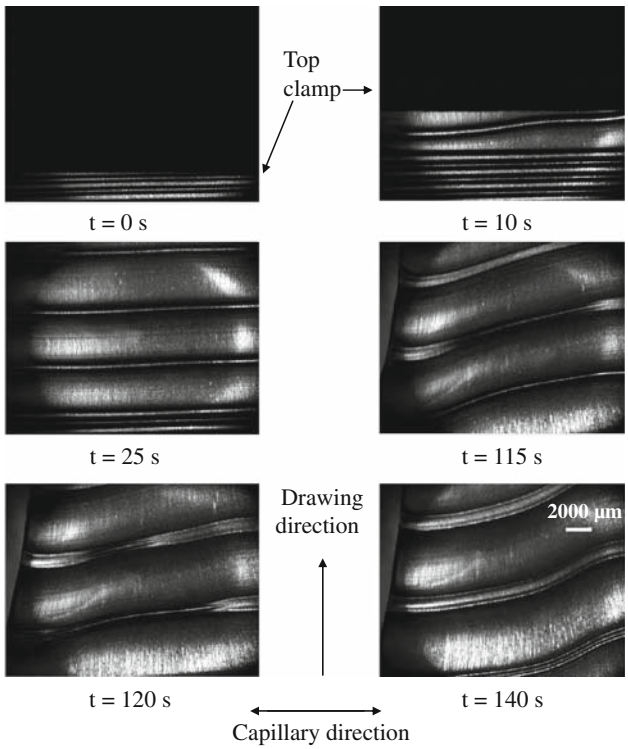

Fig. 18 Optical photographs for the transverse drawing of high-voidage MCF showing the sequential necking of individual micro-capillary walls. Crosshead velocity = 5 mm/s and T = 20 °C

the thin wall regions of the MCF and these regions deform and neck first; subsequently the thicker regions between adjacent capillaries also draw down. In Fig. 20 region 1 is the drawn thin wall section and region 2 is the thicker region between adjacent capillaries. The X-ray data shown in Fig. 22 and Table 3 demonstrate orientation levels in the final film. The X-ray data show that there is a high level of orientation along the draw areas, resulting from deformation in both the thin and thicker sections of the ultra-high voidage MCF.

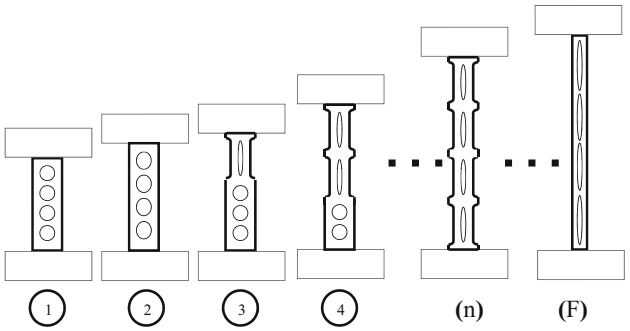

Fig. 19 Schematic diagram showing successive necking of capillary walls during the drawing process: 1. Initial MCF, 2. Elastic deformation, 3. 1st capillary neck, 4. 2nd capillary neck, n. nth capillary neck, F. final necking of material between capillaries. Positions 1-F shown in Fig. 17 of stress–strain curve

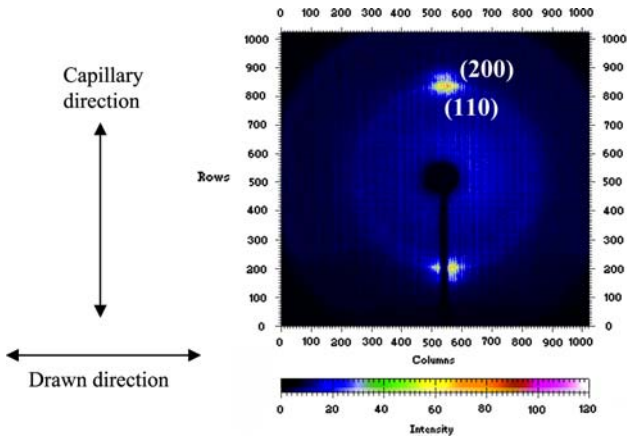

Fig. 22 Indexed WAXS of ultra-high voidage capillaries

The formation of very thin wall ultra-high voidage MCF has clear potential for example in membrane application, provided the base material has micro- or nano-porosity. In addition, ultra-high voidage MCF could be useful as a material from which microreactors could be fabricated; the thin walls would allow high rates of heat transfer and also a clear view of any processes happening within the capillaries due to the high degree of optical transparency.

Physical insight into orientation and deformation behaviour

In terms of low-voidage MCF processing, Fig. 23 shows schematically the primary melt deformation stage. Molten polymer exits the extrusion die containing a certain level of orientation [26] whereupon extrudate swell then occurs, thus reducing both stress levels and orientation. The melt is then drawn down to form a molten film, and solidification of this film occurs when it contacts the chill rollers. The residence time between exiting the die and quenching between the rollers is typically of order one second, and this appears to be sufficiently long to allow molecular relaxation to occur because the resulting low voidage MCF is essentially isotropic as seen from X-ray data in Fig. 10a. Because the low-voidage MCF is initially isotropic, it can subsequently be mechanically drawn by a necking mechanism where orientation subsequently develops along the MCF capillary direction as shown in the X-ray of Fig. 10b.

High-voidage MCF processing produces a different microstructure. This process is shown schematically in

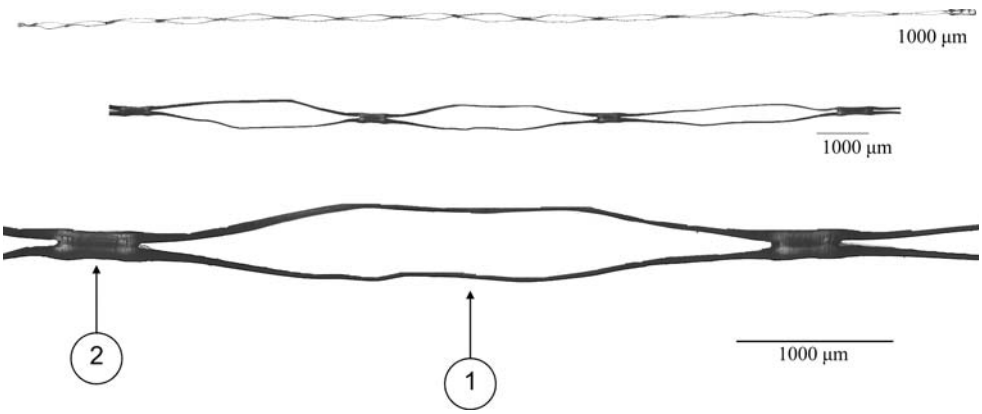

Fig. 20 Optical cross sectional view of ultra-high voidage MCF. Region 1 corresponds to the thin wall section and region 2 to the region between adjacent capillaries

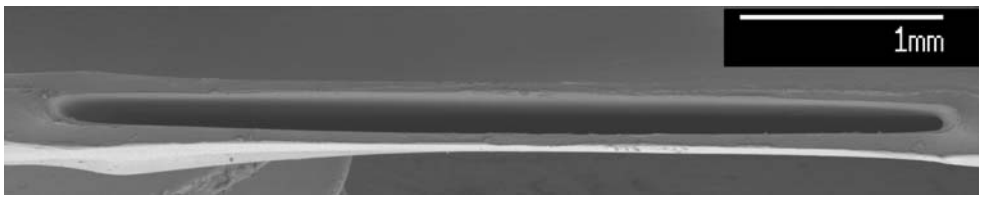

Fig. 21 SEM of the ultra-high voidage MCF

Table 3 Orientation function for the (110) and (200) ultra-high voidage LLDPE

Ultra-high voidage MCF	
Plane	Orientation function f_H
(110)	−0.25
(200)	−0.32

Fig. 24. The key difference from the low-voidage MCF process is the high-speed air quench jets at the die exit. This rapid cooling of the molten polymer at the die exit causes orientation to be frozen into the film during drawing and before relaxation can occur. Subsequent second stage drawing of the high voidage MCF is influenced by the orientation within the material. Axial drawing is limited to brittle fracture but large deformation transverse drawing is possible through a series of successive neck drawing from each capillary. The initial axial orientation of the high-voidage MCF does not impede the transverse drawing and the result demonstrates in general that neck drawing is possible for initially unoriented material or transverse drawing of oriented material. Necking cannot be achieved by second stage axial drawing of oriented material.

Conclusions

This paper has demonstrated that it is possible to control both capillary size and voidage within MCFs by necking deformation of the MCF. The drawing behaviour is sensitive to molecular orientation and this has been quantified using X-ray diffraction.

Low-voidage MCFs were processed in a way that gave little initial orientation in the final film. This results in an MCF that can be axially drawn where necking occurs and a substantial reduction in capillary diameter can be achieved. As anticipated, the drawn film becomes anisotropic.

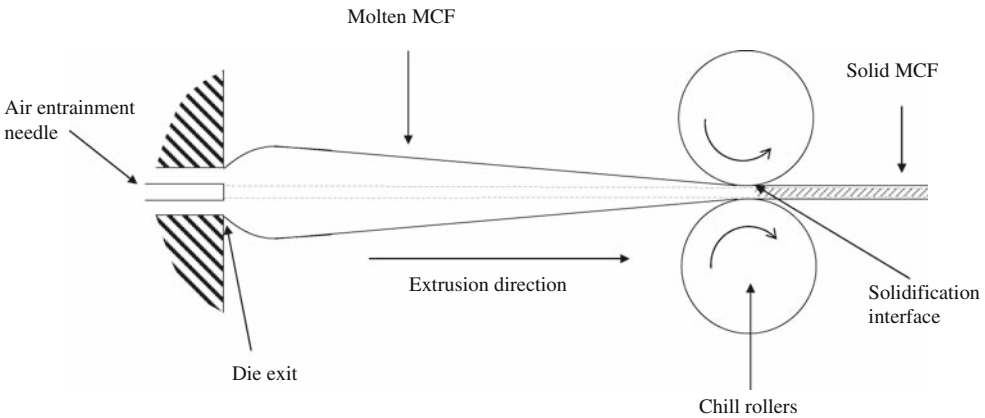

Fig. 23 Extrusion of low-voidage MCF showing the formation of the molten and solid MCF at chill rollers

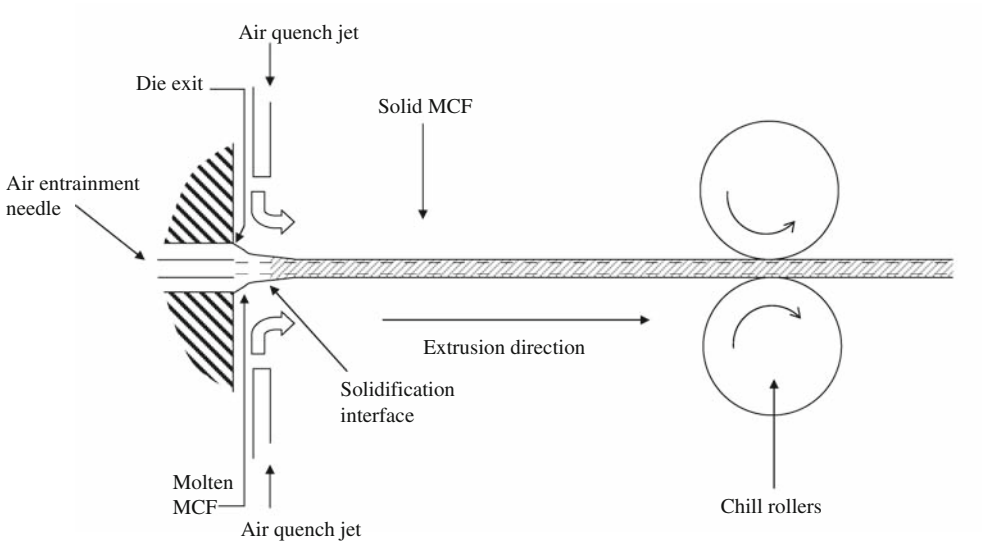

Fig. 24 Extrusion of high-voidage MCF showing rapid cooling of the molten polymer and upstream solidification

By modifying the process conditions, *high-voidage MCFs* can be achieved and these films contain intrinsic orientation. This results in highly anisotropic deformation behaviour of the subsequent film. The high-voidage MCF is brittle when drawn in the axial extrusion direction but draws in an unexpected and unusual way when drawn in the transverse direction. *Ultra-high voidage MCFs* can be produced by transverse drawing when initially there is necking within the thin sections of the MCF but not in the thicker sections, between adjacent capillaries. Subsequently the thicker sections also draw down.

Both capillary size and voidage control are key issues in relation to potential application of MCFs and this paper demonstrates that, for LLDPE, control is possible. As demonstrated using PEU, it can be anticipated that other materials will behave differently as the final geometry, shape and size are very sensitive to both the polymer drawing and orientation behaviour.

Acknowledgements Financial support from EPSRC (Polymer Process Innovation) and CONACyT are gratefully acknowledged.

References

1. Hallmark B, Mackley MR, Gadala-Maria F (2005) Adv Eng Mater 7(6):545. doi:10.1002/adem.200400154
2. Briston JH, Katan LL (1974) Plastics films. The Plastics Institute, London
3. Han CD (1976) Rheology in polymer processing. Academic Press Inc., New York
4. Zatloukal M, Vlcek J (2006) J Non-Newt Fluid Mech 133(1):63. doi:10.1016/j.jnnfm.2005.11.004
5. Dees JR, Spruiell JE (1974) J Appl Polym Sci 18(4):1053. doi:10.1002/app.1974.070180408
6. White J, Cakmak M (1986) Adv Polym Technol 6(3):295. doi:10.1002/adv.1986.060060307
7. Syang-Peng R (2001) J Appl Polym Sci 82(12):2896. doi:10.1002/app.2145
8. Mills NJ, Zhu HX (1999) J Mech Phys Solids 47(3):669. doi:10.1016/S0022-5096(98)00007-6
9. Zhu HX, Mills NJ, Knott JF (1997) J Mech Phys Solids 45(11–12):1875. doi:10.1016/S0022-5096(97)00027-6
10. Hallmark B, Gadala-Maria F, Mackley MR (2005) J Non-Newt Fluid Mech 128(2–3):83. doi:10.1016/j.jnnfm.2005.03.013
11. Hornung CH, Mackley MR, Baxendale IR, Ley SV (2007) Org Process Res Dev 11(3):399. doi:10.1021/op700015f
12. Hornung CH, Hallmark B, Hesketh RP, Mackley MR (2006) J Micromech Microeng 16(2):434. doi:10.1088/0960-1317/16/2/030
13. Jiang PX, Fan MH, Si GS, Ren ZP (2001) Int J Heat Mass Transfer 44(5):1039. doi:10.1016/S0017-9310(00)00169-1
14. Ward IM (1983) Mechanical properties of solid polymers. Wiley, Bristol
15. Lamberti G, Titomanlio G, Brucato V (2001) Chem Eng Sci 56(20):5749. doi:10.1016/S0009-2509(01)00286-X
16. Bashir Z, Keller A (1989) Colloid Polym Sci 267(2):116. doi:10.1007/BF01410349
17. Ward IM (1962) Proc Phys Soc 80:1176. doi:10.1088/0370-1328/80/5/319
18. Vincent PI (1960) Polymer (Guildf) 1:7. doi:10.1016/0032-3861(60)90003-3
19. Robertson RE (1964) General Electric Co. Report No. 64-RL-358OC
20. Zhang XM, Elkoun S, Ajji A, Huneault MA (2004) Polymer (Guildf) 45(1):217. doi:10.1016/j.polymer.2003.10.057
21. Hallmark B, Medina DI, Mackley MR (2007) In: Proceedings of PPS-23 polymer processing society. Salvador, Brazil
22. Hammersley AP, Svensson SO, Thompson A, Graafsma H, Kvick A, Moy JP (1995) Rev Sci Instrum 66(3):2729. doi:10.1063/1.1145618
23. Bunn CW (1939) Trans Faraday Soc 35:482. doi:10.1039/tf9393500482
24. Schrauwen BAG, Von Breemen LCA, Spoelstra AB, Govaert LE, Peters GWM, Meijer HEH (2004) Macromolecules 37(23):8618. doi:10.1021/ma048884 k
25. Hermans PH (1946) Contributions to the physics of cellulose fiber. Elsevier, Amsterdam
26. Liang RF, Mackley MR (2001) J Rheol 45(1):211. doi:10.1122/1.1332786